Numerical Modeling of Laminar Flame Speed and Autoignition Delay Using General Fuel-Independent Function

Filip Jurić[a], Marko Ban[b], Peter Priesching[c], Carsten Schmalhorst[d], Neven Duić[a], Milan Vujanović[a, *]

[a] University of Zagreb, Faculty of Mechanical Engineering and Naval Architecture, Ivana Lučića 5, 10000 Zagreb, Croatia

[b] SDEWES Centre, Ivana Lučića 5, 10000 Zagreb, Croatia

[c] AVL List GmbH, Alte Poststraße 152, 8020 Graz, Austria

[d] AVL Deutschland GmbH, Frankfurter Ring 213, 80807 Munich, Germany

[*] Corresponding author e-mail: milan.vujanovic@fsb.hr

ABSTRACT

The impact of the transport sector on climate change and carbon dioxide emissions into the atmosphere can be decreased by the utilization of biofuels and e-fuels. The chemical kinetics for calculating the combustion process of new biofuels and e-fuels is often excessively computationally demanding for numerical simulations, leading to the development and employment of combustion models, such as flamelet models. Such models require precalculated data of laminar flame speed and autoignition timing. The developed procedure in this work scrutinizes available reaction mechanisms of several fuels with the validation against existing experimental data of autoignition and laminar flame velocities, aiming for the generation of lookup databases. The autoignition of fuel/air mixtures for different conditions is pre-tabulated from nondimensional calculations of constant pressure reactor. Simultaneously,

[*] Corresponding author

the laminar flame speed is pre-tabulated from premixed freely propagating reactors, for which calculation chemical kinetics software are applied. The ignition delay of cold flame and primary ignition was calculated using inflection point criteria implemented in the proposed method. The developed imputations method is based on the lognormal distribution for laminar flame speed in equivalence ratio direction and exponential functions for pressure, temperature, and exhaust gas recirculation directions. The laminar flame speed and autoignition databases generation procedure was demonstrated on prospective e-fuel three-oxyethylene dimethyl ether (OME-3) fuel by validating the available mechanism against the experimental data. Finally, the generated databases are implemented into the computational fluid dynamics software and verified with the detailed chemical mechanism of OME-3 fuel.

KEYWORDS

Laminar flame speed; autoignition; flamelet model; chemical kinetics; combustion; e-fuels

1. INTRODUCTION

One way to mitigate the transport sector's impact on climate change and carbon dioxide emissions into the atmosphere is the utilization of biofuels and e-fuels in the transport sector [1]. Therefore, the implementation of biofuels [2] and e-fuels [3] in conventional internal combustion engines is of great importance to accelerate the transition of the transport sector to renewable energy sources. One approach to achieving greener transport [4] and the energy sector [5] is the application of biofuels. The impact on the generation of emissions such as nitrogen oxides is still not fully explored. Therefore, numerous researches are conducted to obtain biofuel impact on emissions when they substitute conventional fuel in existing combustion systems [6]. Other modern approaches are the implementation of alternative fuels, such as ammonia and its blends with natural gas [7], synthesized kerosine from coal [8], and

gasoline substitutes like ethanol in passenger car engines [9] and marine engines[10], and toluene reference fuel [11].

There are already numerous biofuels and e-fuels, some similar and some less to conventional petrol and diesel fuels, but each with different physical properties, chemistry kinetics, and combustion characteristics [12]. In order to predict the fuel combustion under different fuel/air mixtures, loads, and temperatures, Computational Fluid Dynamics (CFD) with the chemical kinetics or combustion models are commonly employed [13]. The chemical kinetics is often too computationally demanding for numerical simulations, leading to the frequent use of combustion models, such as coherent flame models [14]. In coherent flame models, ignition delay and laminar flame velocities for different operating conditions must be precalculated in the form of a database or correlation formula [15]. The standard correlations for new biofuels and e-fuels are not accurate enough to validate their combustion process, primarily the low-temperature auto-ignition phenomenon [16]. In [17], the correlation functions between autoignition timing and flame speed propagation were developed based on the temperature gradients measured from the rapid compression.

Correlation functions for the autoignition of biodiesel fuels that feature ignition of fuel-air mixtures at high temperatures and their validation with the chemistry kinetic mechanisms were presented by the authors in [18], where the excellent agreement between the previously published mechanism was achieved. The dependency of autoignition timing and pollutant emissions results was demonstrated in [19], where the convenient diesel fuels with some percentage of biodiesel were observed at high-temperature conditions. The investigation results are that the rise in the ambient temperature lowers the ignition delay for all diesel fuel, which was expected. Recent publications have also investigated the investigation of biodiesel fuels produced by different sources [20]. For example, the autoignition delay of microalgae biodiesel blends was investigated numerically to determine combustion efficiency and pollutant

emissions [21]. Additionally, an experimental autoignition investigation of biodiesel produced from the plant oil and its impact on the combustion process inside a compression ignition engine was observed [22]. The results showed that the biodiesel blend at 20% of the content exhibited better combustion performance and emission characteristics than other blend proportions.

In [23], the authors performed an experimental optical study of biodiesel ignition delay, where the correlation between autoignition timing and combustion process was demonstrated. A similar approach for determining the influence of pollutant concentrations of nitrogen oxides and carbon monoxide on autoignition timing under different exhaust gas recirculation (EGR) mass fractions was examined by the authors [24], where the diesel fuel with a small share of biodiesel was used. For the internal combustion engine operating conditions, a numerical method named spherically expanded flames was used to determine the autoignition and laminar flame speed propagation for a different share of e-fuel (dimethyl-ether), air, and helium [25]. The simulation results adequately captured the physics of unsteady flame propagation, autoignition, and the controlling reactions, but not at the early ignition stages.

Lately, the penetration of machine learning techniques has accelerated enormously in all science areas, so in this area too. Rahnama et al. [26] proposed the machine learning neural network for fuel consumption reduction in internal combustion engines, where the start of injection and its influence on autoignition timing was observed. Deep neural networks for internal combustion engines were also employed to determine emissions from the biodiesel combustion process [27]. In [28], the authors published the results of dual-fuel autoignition, which were predicted by the machine learning technique. The sensitivity analysis showed that the fuel ratio between the primary and secondary fuels has the most significant effect on dual-fuel ignition. Furthermore, an exciting approach, similar to the developed procedure in this work, was published by the authors of [29], where the calculation of the autoignition and laminar flame speed was modeled by ignition to propagation reduced scheme, which was

upgraded to additionally calculate the autoignition timing. Another approach that aims to obtain laminar flame speed with general formula is presented in [30]. The authors introduced a term that depends on polynomial, exponential factors, with additional constant defined from the precomputed database. Additionally, the same procedure was applied for obtaining ethanol/gasoline blends databases, where high accuracy in correlation is achieved [31]. Other researchers tend to determine laminar flame speed correlations for a single fuel. In [32], the authors proposed correlation functions for surrogate gasoline fuels as an exponential function in temperature and pressure direction. An exceptional scientific contribution was conducted to developing correlation functions of hydrogen fuel for spark ignition operating conditions [33]. Furthermore, additional research has been undertaken to develop correlation functions capable of describing hydrogen mixture with gasoline [34] and methanol [35] for combustion inside spark-ignition engines.

In this work, the effects of complex chemistry kinetics are reproduced by developing efficient database creation consisting of the relevant ignition data used by existing combustion models. In the pre-processing stage, available reaction mechanisms of several fuels were investigated and validated against existing experimental data of autoignition and laminar flame velocities. The autoignition of fuel/air mixtures for different conditions is pre-tabulated from nondimensional constant pressure reactor calculation. At the same time, the laminar flame speed is pre-tabulated from premixed freely propagating reactors, for which the LOGEsoft™ and Cantera open-source software were used. The ignition delay of cold flame and main ignition was calculated using the inflection point criteria presented in [35] and implemented in the proposed method. The data imputation and extrapolation method was developed as a general fuel-independent function. The nonlinear least squares algorithm was employed to fill the unsuccessfully calculated points of databases in the post-processing.

In this work, the novel general, fuel-independent procedure is developed and implemented into CFD software based on the lognormal distribution for laminar flame speed in equivalence ratio direction and exponential functions for pressure, temperature, and exhaust gas recirculation directions. Three parameters are used to determine the dependence of the laminar flame speed or autoignition results on pressure and equivalence ratio directions. Additionally, the method is also applicable to dual-fuel combustion. The ignition delay and laminar flame speed values of fuel blends are described with the additional parameter of the fuel composition. Finally, the database implementation is verified with the detailed chemical mechanism of complex internal combustion operating case in computational fluid dynamics and validated with experimental data.

2. MATHEMATICAL MODEL

In this section, the mathematical model for calculating the correlation function and models used in the validation and verification are presented. For chemistry calculation, commercial LOGEsoft™ and Cantera open-source software were used, while for CFD simulation AVL FIRE™ was used.

2.1. Laminar flame speed

For the definition of the correlation function of the laminar flame speed points, firstly, the calculation on chemistry solvers was performed. The chemistry solver calculations were defined with the four-dimensional grid: temperature, pressure, equivalence ratio, and EGR. The calculations were performed on premixed freely propagating reactors, where each combination of four previously mentioned parameters was calculated as a separated reactor. The raw calculated data were sorted in the five-dimensional matrix, on which the correlation function is performed.

Figure 1 shows the procedure of the developed method for the generation of a laminar flame speed database for the coherent flame models.

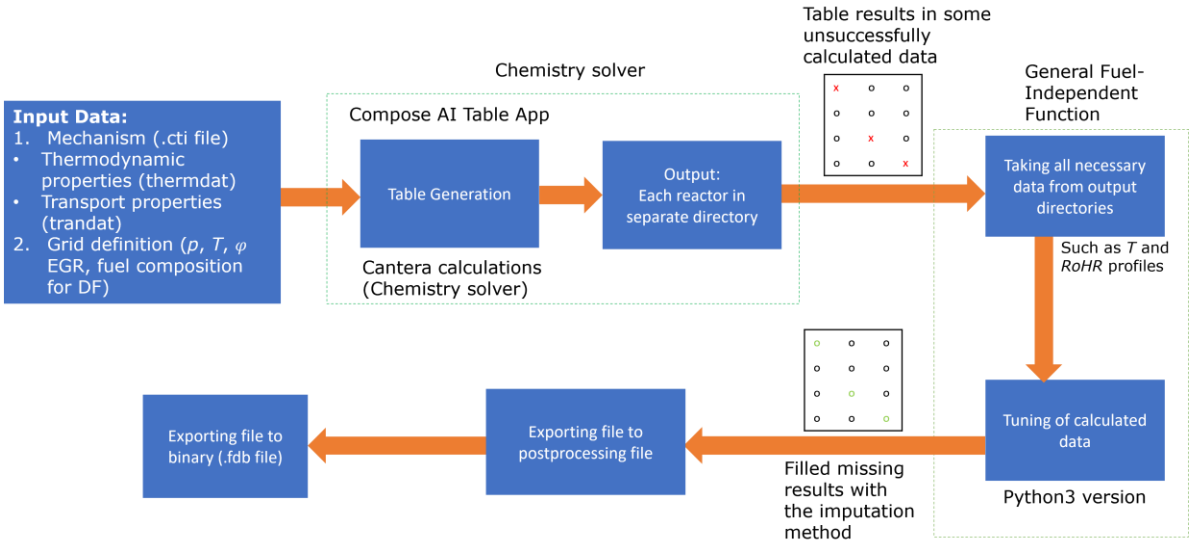

Figure 1 Flowchart of the developed procedure for generation of laminar flame speed and autoignition databases

The correlation function was tuned for calculated data, which was defined as the lognormal distribution for equivalence ratio (φ) and as the exponential function for the pressure (p) direction. The tuning equation has the following form:

$$S_L(p,\varphi) = S_{L,ref}\left[\frac{1}{\varphi\sigma\sqrt{2\pi}}\exp\left(-\frac{(\ln\varphi-\mu)^2}{2\sigma^2}\right)\right]\left(\frac{p}{p_{ref}}\right)^{\beta} \quad (1)$$

where μ and σ are two tuning parameters that are calculated for each combination of the temperature and EGR. For the calculation of μ and σ parameters that have the lowest disagreement with the raw computed data, the nonlinear least-squares method was employed with the Levenberg-Marquardt algorithm. p_{ref} is reference pressure of 0.1 MPa, while $S_{L,ref}$ is referent laminar flame speed at selected calculated point, which was in this case at equivalence ratio 1, and pressure 0.1 MPa. The algorithm was based on SciPy open-source package and its function

scipy.optimize.least_squares that accounts for the optimized parameters of general function for each temperature point. In order to obtain the optimized parameters, the objective function is defined as:

$$f_{S_L} = \min \sum_{i=1}^{m} \left[S_{L_i} - S_L(p_i, \varphi_i) \right]^2 \tag{2}$$

where S_{L_i} is the calculated laminar flame speed from the chemistry solver, and *m* is the number of points used for obtaining the formula of laminar flame speed. The objective function is approximated by the linearization in each iteration step. The φ is changed with the estimation $\varphi + \delta$, and to determine δ the following term has to be calculated:

$$f_{S_L} \approx S_L(p_i, \varphi_i + \delta) + \frac{\partial S_L(p_i, \varphi_i)}{\partial \varphi} \delta \tag{3}$$

2.2. Autoignition timing

For the definition of the correlation function of the autoignition points, firstly, the calculation on chemistry solvers was performed. The chemistry solver calculations were also defined with the four-dimensional grid, where the parameters were temperature, pressure, equivalence ratio, and EGR, the same as in the laminar flame speed calculations. The calculations were performed on nondimensional, perfectly stirred reactors, where each combination of four previously mentioned parameters was calculated as a separated reactor. The raw calculated data were sorted in the eight-dimensional matrix, where the four additional output parameters were autoignition timing, cold flame autoignition timing, released heat, and heat released by cold flame. The procedure of the developed method for generating the autoignition (τ) database is similar to the laminar flame speed database for the coherent flame models.

$$\tau(p,\varphi) = \tau_{ref}\left(\frac{p}{p_{\mathrm{ref}}}\right)^{\alpha}(\varphi)^{\beta} \tag{4}$$

where α and β are two tuning parameters calculated for each combination of the temperature and EGR. For the calculation of α and β parameters that have the lowest disagreement with the raw calculated data, the nonlinear least-squares method was employed with the Levenberg-Marquardt algorithm. The objective function is defined as

$$f_{\tau} = \min \sum_{i=1}^{m} [\tau_i - \tau(p_i,\varphi_i)]^2 \tag{5}$$

Where the objective function is approximated by the linearization in each iteration step. The φ is changed with the estimation $\varphi + \delta$, and to determine δ the following term has to be calculated:

$$f_{\tau} \approx \tau(p_i,\varphi_i + \delta) + \frac{\partial \tau(p_i,\varphi_i)}{\partial \varphi}\delta \tag{6}$$

As in the case of the laminar flame speed algorithm was set to bisquare robust regression.

2.3. Coherent flame model – ECFM-3Z

An alternative to modeling combustion via chemical kinetics is using a coherent flame model suitable for simulating combustion inside diesel engines. One of such models is the extended coherent flame model in 3 zones (ECFM-3Z). It has a decoupled treatment of chemistry and turbulence [36].

In the model, the following equation is solved for the flame surface density Σ:

$$\frac{\partial \Sigma}{\partial t} + \frac{\partial}{\partial x_j}\left(\bar{u}_j \Sigma\right) - \frac{\partial}{\partial x_j}\left(\frac{\nu_t}{Sc_t}\frac{\partial \Sigma}{\partial x_j}\right) = S_\Sigma \tag{7}$$

where t is time, x_j are Cartesian coordinates, $\bar{u}_j$ is averaged velocity in Cartesian coordinates, ν_t is the turbulent kinematic viscosity, Sc is unidimensional Schmidt number, and S_Σ is the source term in which laminar flame speed contribution is added through three phenomena, flame propagation, flame destruction and flame straining. In the model, transport equations for the following species are solved: O_2, N_2, NO, CO_2, CO, H_2, H_2O, O, H, N, OH:

$$\frac{\partial \bar{\rho}\tilde{Y}_X}{\partial t} + \frac{\partial \bar{\rho}\tilde{u}_i\tilde{Y}_X}{\partial x_i} = \frac{\partial}{\partial x_i}\left(\left(\frac{\mu}{Sc} + \frac{\mu_t}{Sc_t}\right)\frac{\partial \tilde{Y}_X}{\partial x_i}\right) + \overline{\dot{\omega}}_X \tag{8}$$

Where $\overline{\dot{\omega}}_X$ is the average combustion source term and $\tilde{Y}_X$ is the average mass fraction of species X, while $\bar{\rho}$ is averaged density. The fuel is divided into two parts: the unburned ($\tilde{Y}_{Fu}^u$) and burned ($\tilde{Y}_{Fu}^b$) fuel. For both of them, additional transport equations are solved:

$$\frac{\partial \bar{\rho}\tilde{Y}_{Fu}^u}{\partial t} + \frac{\partial \bar{\rho}\tilde{u}_i\tilde{Y}_{Fu}^u}{\partial x_i} = \frac{\partial}{\partial x_i}\left(\left(\frac{\mu}{Sc} + \frac{\mu_t}{Sc_t}\right)\frac{\partial \tilde{Y}_{Fu}^u}{\partial x_i}\right) + \bar{\rho}\tilde{\dot{S}}_{Fu}^u + \overline{\dot{\omega}}_{Fu}^u - \overline{\dot{\omega}}_{Fu}^{u\to b} \tag{9}$$

$$\frac{\partial \bar{\rho}\tilde{Y}_{Fu}^b}{\partial t} + \frac{\partial \bar{\rho}\tilde{u}_i\tilde{Y}_{Fu}^b}{\partial x_i} = \frac{\partial}{\partial x_i}\left(\left(\frac{\mu}{Sc} + \frac{\mu_t}{Sc_t}\right)\frac{\partial \tilde{Y}_{Fu}^b}{\partial x_i}\right) + \bar{\rho}\tilde{\dot{S}}_{Fu}^b + \overline{\dot{\omega}}_{Fu}^b + \overline{\dot{\omega}}_{Fu}^{u\to b} \tag{10}$$

where $\tilde{\dot{S}}_{Fu}^u$ is a source term representing fuel evaporation. $\overline{\dot{\omega}}_{Fu}^u$ and $\overline{\dot{\omega}}_{Fu}^b$ represent oxidation of (un)burned fuel, while $\overline{\dot{\omega}}_{Fu}^{u\to b}$ represents fuel mass transfers between various zones. μ and μ_t are laminar and turbulent dynamic viscosity.

The combustion area can be divided into three zones: a pure fuel zone, a pure air plus possible EGR zone, and mixed air and fuel zone. The model describes autoignition and premixed and diffusion flames. A schematic showing these zones is shown in Figure 2 [37].

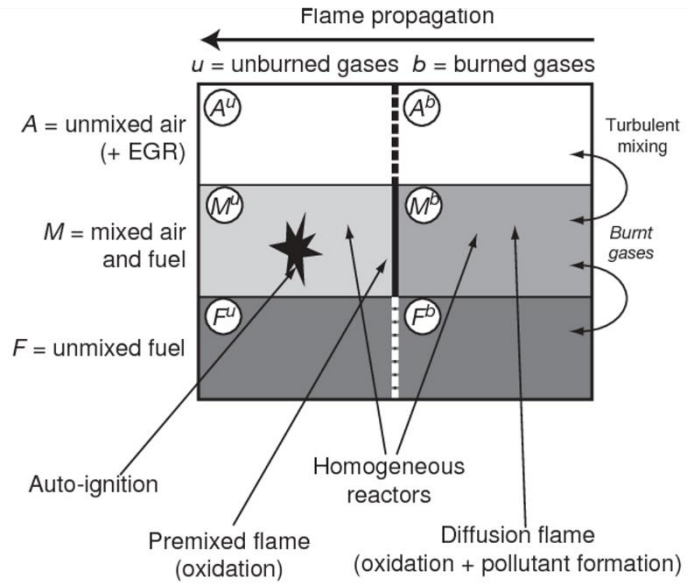

Figure 2 Schematic of the ECFM-3Z model cell [37]

3. VALIDATION

For the validation of the calculated data from chemistry solvers, four mechanisms of e-fuel OME-3 were compared with the experimental data: Cai et al. [16], Ren et al. [38], Sun et al. [39], and Lin et al. [40]. Figure 3 shows the calculated laminar flame results at a pressure of 0.1013 MPa and temperature of 408 K, and with four previously mentioned chemical mechanisms, where good agreement was achieved with all data.

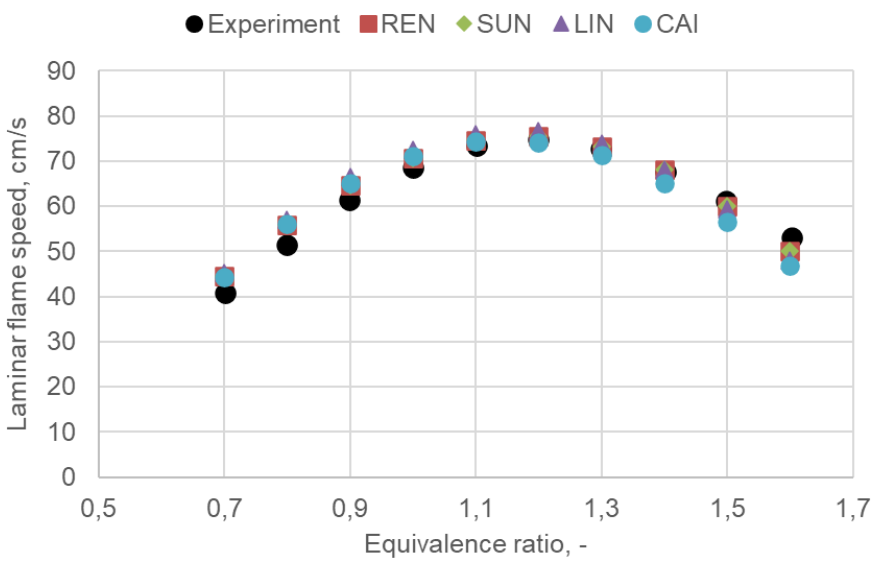

Figure 3 Comparison of calculated laminar flame speed with four chemical mechanisms and experimental data at 0.1013 MPa and 408 K

For the exact mechanism, the validation of results was performed on the autoignition results, where the best agreement with experimental data was achieved with the Lin et al. mechanism. The autoignition results were performed in Figure 4, where the results are shown at the pressure of 2 MPa for equivalence ratio values of 0.5, 1.0, and 2.0. The experimental autoignition results are taken from [16]. According to the performed validation, the Cai et al. chemical mechanism was selected to further investigate the correlation function since it features the highest number of chemical reactions and chemical species.

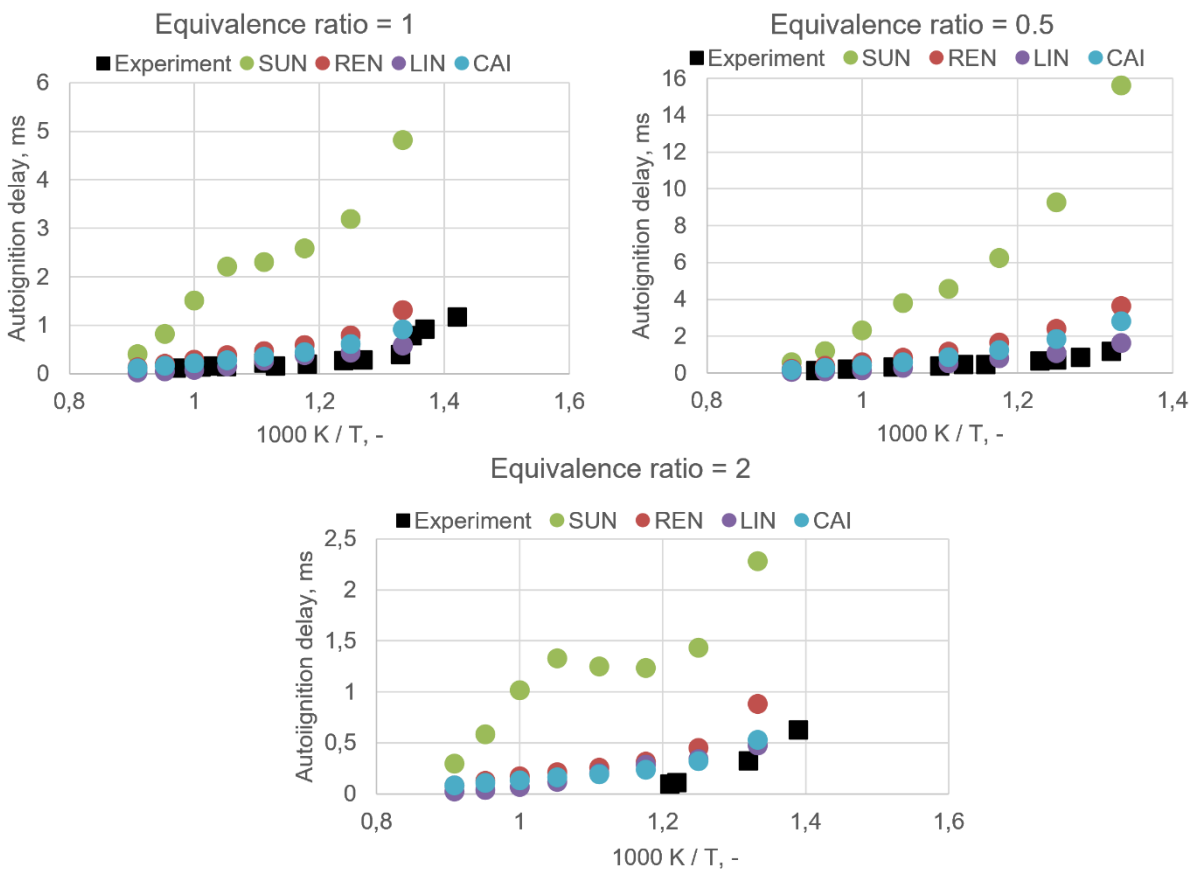

Figure 4 Comparison of calculated autoignition data with four chemical mechanisms and experimental data at 2 MPa for equivalence ratios: 0.5, 1.0 and 2.0

4. NUMERICAL SETUP

This chapter presents the numerical setup of the verification case for generated laminar flame speed and autoignition tables of OME-3 fuel. The verification case was performed on Volvo I5D engine, for which the detailed description of mesh dependency is available in [13]. The engine and injector data are shown in Table 1.

Table 1 Engine and injector specifications

Engine data	
Bore	81 mm

Stroke	93.15 mm
Connecting rod length	147 mm
Compression ratio	16.5 : 1
Displacement	2.4 dm^3
Number of cylinders	5
Injector data	
Number of nozzle holes	7
Spray cone angle	145°
Flow rate (at 100 bar Δp)	440 cm^3 / 30 s
The shape of the nozzle dome	Micro Sac

The calculation of a moving computational mesh shown in Figure 5 was generated with the defined boundary selections. Due to the cyclic symmetry, the computation mesh is the cylinder part that features a single nozzle hole. Mesh details, like volume and number of cells, are given in Table 2. In Table 3, the boundary conditions of the engine operating cases are shown.

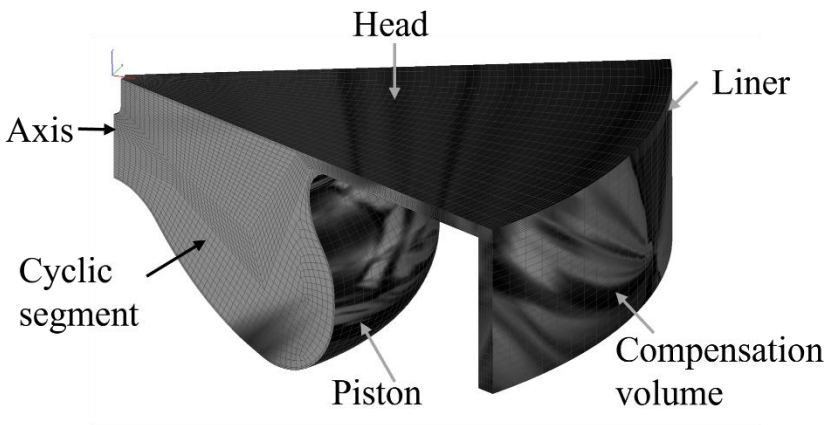

Figure 5 Boundary selections of the computational mesh

Table 2 Mesh details

	Top Dead Centre	**Bottom Dead Centre**
Volume, cm^3	4.67	75.88
Number of cells	54 663	112 854

Table 3 Boundary conditions for the verification operating case

Face selection	**Boundary Condition**
Piston	Type: Wall Temperature: 473 K
Liner	Type: Wall Temperature: 423 K
Axis	Type: Symmetry
Segment	Type: Inlet/Outlet
Compensation volume	Type: Wall, Mesh movement
Head	Type: Wall Temperature: 443 K

In Table 4, injection parameters for two observed operating cases are shown. Two cases that feature single and multi-injection strategies are selected in order to prove the capability of valid autoignition and combustion process modeling for both modeling strategies.

Table 4 Injection parameters for the verification operating cases

	Multi injection	**Single injection**
Injected mass	0.4, 0.4, 5.8, 0.8 mg	4.12 mg
Injection timing	683.9 - 740.7 °CA	718.2 - 731.3 °CA

For the time discretization, an automatic time step was used, where the maximum value of the local CFL number was set to 1. For the calculation of the spray process, the Euler Lagrangian model was used [41], with the Wave breakup model [42] and Abramzon evaporation model [43]. The CFD verification simulations are performed using the AVL AST software package, which has implemented the ECFM-3Z model and detail chemistry solvers. In Table 5, the grid definition of generated lookup databases for CFD implementation is given.

Table 5 Grid definition for laminar flame speed and autoignition timing databases

Laminar flame speed	**Grid points**
Temperature, K	300, 400, 500, 600, 700, 800, 900, 1000, 1100, 1250
Pressure, MPa	0.1, 0.2, 0.5, 1, 2, 5, 10, 15, 20, 25, 30
Equivalence ratio, -	0.2, 0.4, 0.6, 0.8, 0.9, 1, 1.1, 1.2, 1.4, 1.6, 1.8, 2, 3, 4, 5
EGR, -	0, 0.2, 0.4, 0.6
Autoignition	**Grid points**
Temperature, K	600, 620, …, 740, 760, 800, 840, …, 1400, 1440, 1500
Pressure, MPa	0.1, 0.2, 0.5, 1, 2, 5, 10, 15, 20, 25, 30
Equivalence ratio, -	0.2, 0.4, 0.6, 0.8, 0.9, 1, 1.1, 1.2, 1.4, 1.6, 1.8, 2, 3, 4, 5
EGR, -	0, 0.1, 0.2, 0.3, 0.4, 0.5, 0.6, 0.7, 0.8

5. RESULTS AND DISCUSSION

In this section, the results of the developed correlation functions and calculated data were compared on three-dimensional and two-dimensional diagrams. Figure 6 shows the calculated and tuned laminar flame speed results with the correlation function in Equation (1) at 1100 K with Cai et al. chemical mechanism. The a) diagram of Figure 6 shows the surface of raw data calculated from the chemistry solver, which is tuned with the correlation function, and where the results at the b) diagram of Figure 6 are obtained.

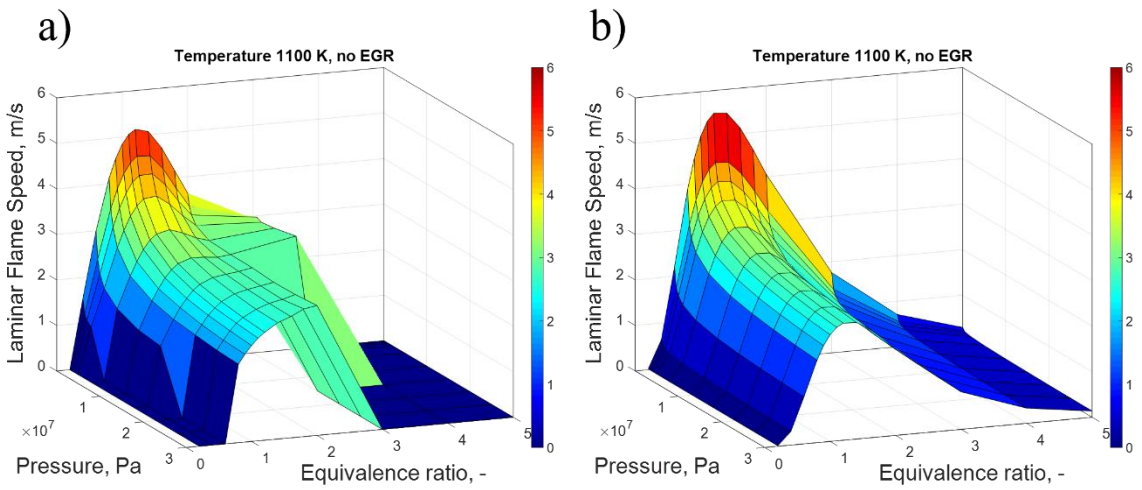

Figure 6 Calculated chemistry solver results (a) and laminar flame speed results with the correlation functions (b) at 1100K

Figure 8 shows the calculated results from the chemistry solver used as input to obtain the shape of laminar flame speed data and the shape obtained by the correlation function procedure on four parameters: temperature, equivalence ratio, pressure, and EGR mass fraction. The calculated laminar flame speed data is shown as the black dots, while the surface shows the results with the correlation function in Equation (1). From Figure 8**Pogreška! Izvor reference nije pronađen.**, a good trend is achieved between calculated results and the results obtained from the general function approach. For the highest temperature, 1250 K, only 6 points are obtained from chemistry solver reactions, compared to the lower temperatures where the chemistry solver is more stable. The general function approach shows a robust extrapolation solution for such cases since it only needs 3 points to determine the whole laminar flame speed shape in pressure and equivalence ratio directions. In Figure 8, the same results for different pressure values. It can be seen that the agreement between the general function approach and calculated data using the conventional Gülder approach for extrapolation [44] is better for the lean mixtures and around the stoichiometric equivalence ratio. At the same time, a more significant discrepancy was achieved for the fuel-rich region.

Figure 9 shows the same results as in Figure 7 for temperature of 800 K, at different pressure values. Additionally, the number of successfully calculated data from the chemistry solver (red circles) is reduced with pressure and equivalence ration increase. Nevertheless, as shown, the general function method shows good robustness with fewer obtained points. Additionally, the method was also validated against calculated laminar flame speeds at different EGR values in Figure 10. With increased EGR, a more significant discrepancy with chemistry solver data is obtained, which has unexpectedly high values in fuel rich regions. Such high values can also be attributed to the drawback of a chemical mechanism not intended to calculate the laminar flame speed for such conditions or to chemistry solver converging deficiency.

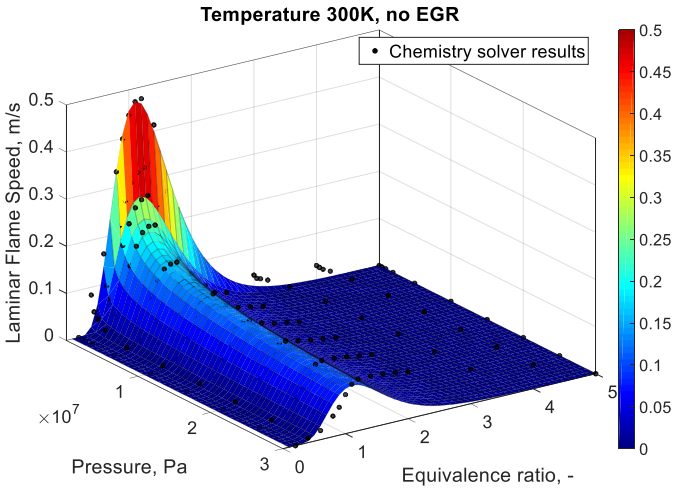
Temperature 300K, no EGR
Chemistry solver results
Laminar Flame Speed, m/s
Pressure, Pa
×10^7
Equivalence ratio, -

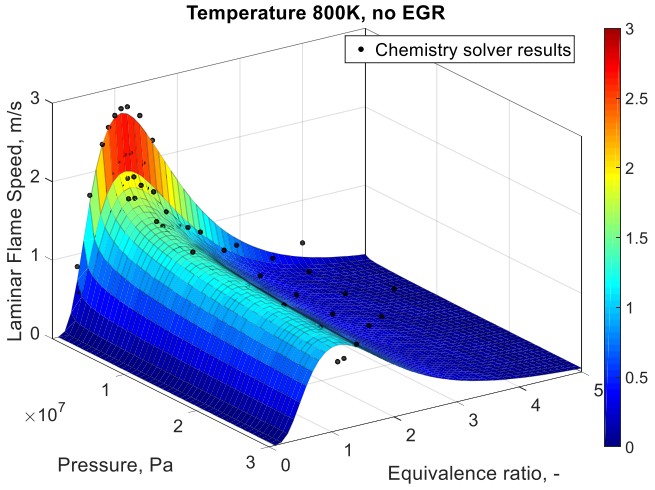
Temperature 800K, no EGR
Chemistry solver results
Laminar Flame Speed, m/s
Pressure, Pa
×10^7
Equivalence ratio, -

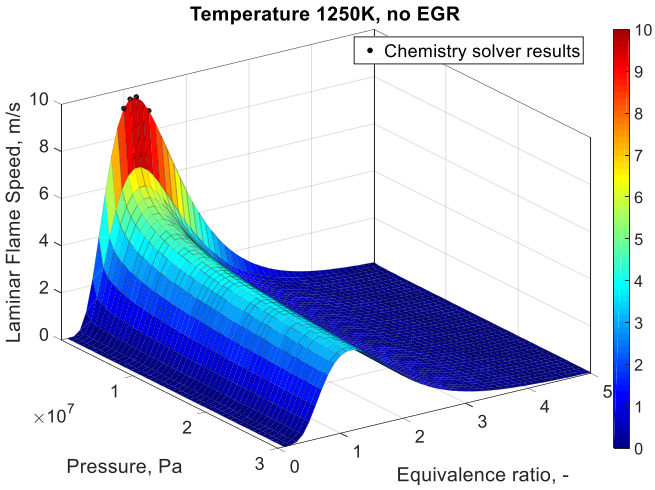
Temperature 1250K, no EGR
Chemistry solver results
Laminar Flame Speed, m/s
Pressure, Pa
×10^7
Equivalence ratio, -

Figure 7 Lminar flame speed results with the correlation functions at 300, 800 and 1250 K and without EGR

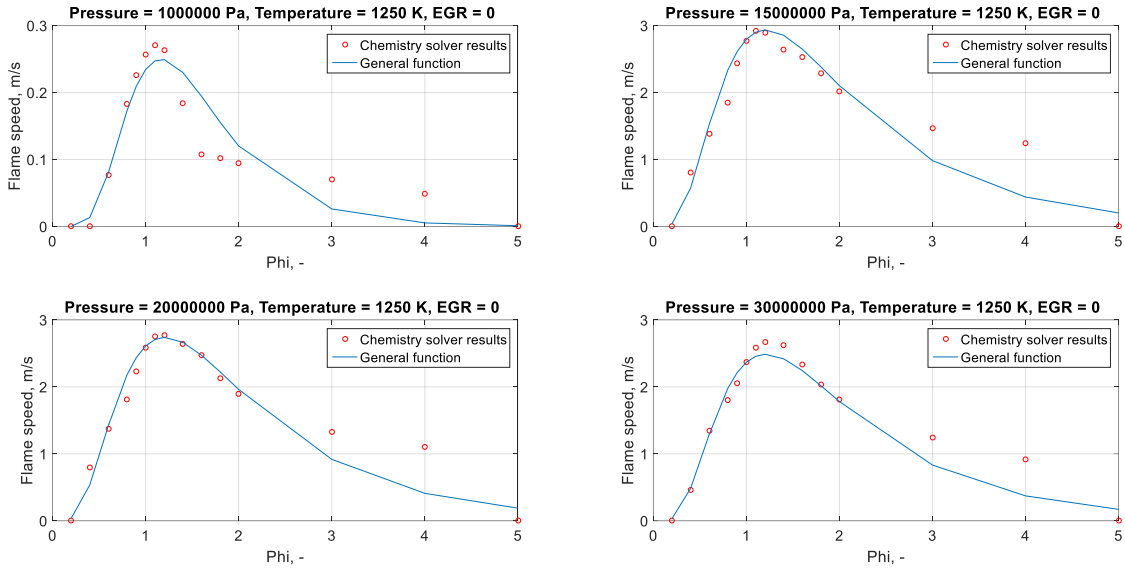

Figure 8 Calculated results with Gülder approach and laminar flame speed results with the correlation function at 1250 K

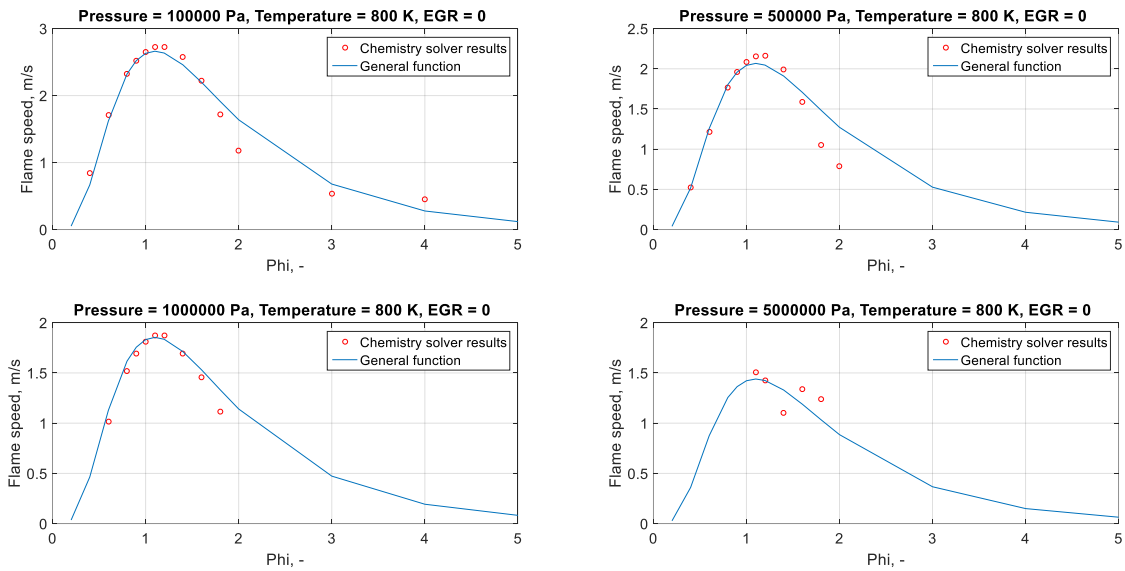

Figure 9 Chemistry solver results and laminar flame speed results with the correlation function at 800 K

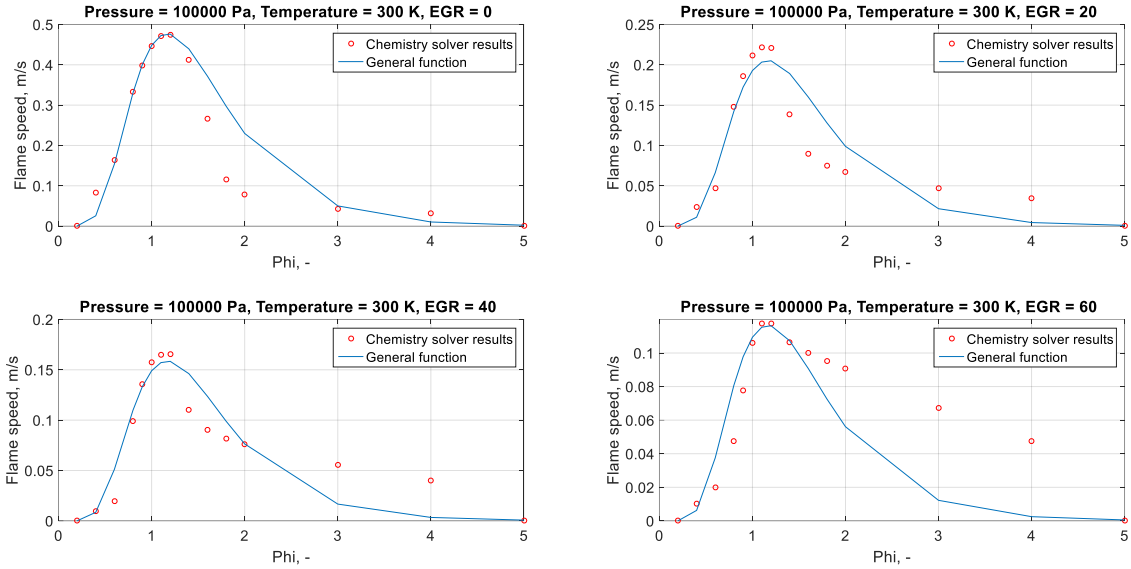

Figure 10 Chemistry solver results and laminar flame speed results with the correlation function at different EGR values

Figure 11 shows the coefficient of determination (R^2) values between the chemistry solver results and general function at different temperatures and EGR values. It can be seen that the best agreement between chemistry solver results and general function is obtained around 500 K. the correlation decreases markedly with the increase of EGR and at high temperatures.

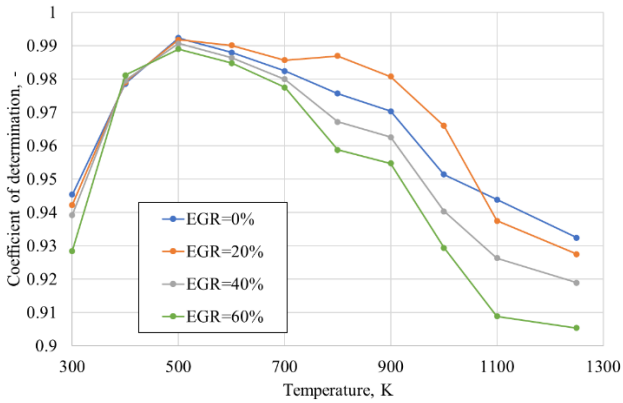

Figure 11 Coefficient of determination values between chemistry solver results and general function for different temperature and EGR values

Pogreška! Izvor reference nije pronađen. Figure 12 shows the calculated and tuned laminar flame speed results with the correlation function in Equation (4) with Cai et al. chemical mechanism. For most autoignition delay time representation, a logarithmic scale is used in order to emphasize that the order of magnitude is sufficient for valid autoignition modeling. In Figure 12, the linear scale emphasizes a good agreement with the chemistry solver results at temperatures 1000 K and 1200 K.

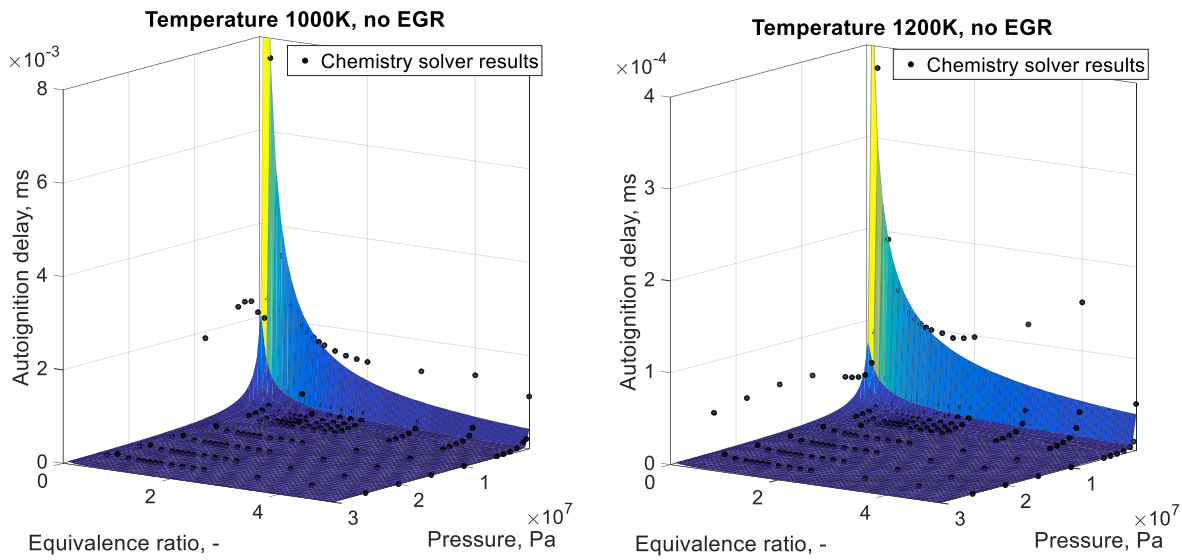

Figure 12 Calculated (black dots) and autoignition timing results with the correlation functions without EGR at 1000 and 1200 K

Figure 13 shows the same results as Figure 12 for 2D cuts at different pressure values. It can be seen that the agreement between the calculated data and obtained results is better for the points around the stoichiometric equivalence ratio and around the fuel-rich region. In contrast, additional efforts are required for the lean air-fuel mixtures and the fuel-rich region at higher pressures.

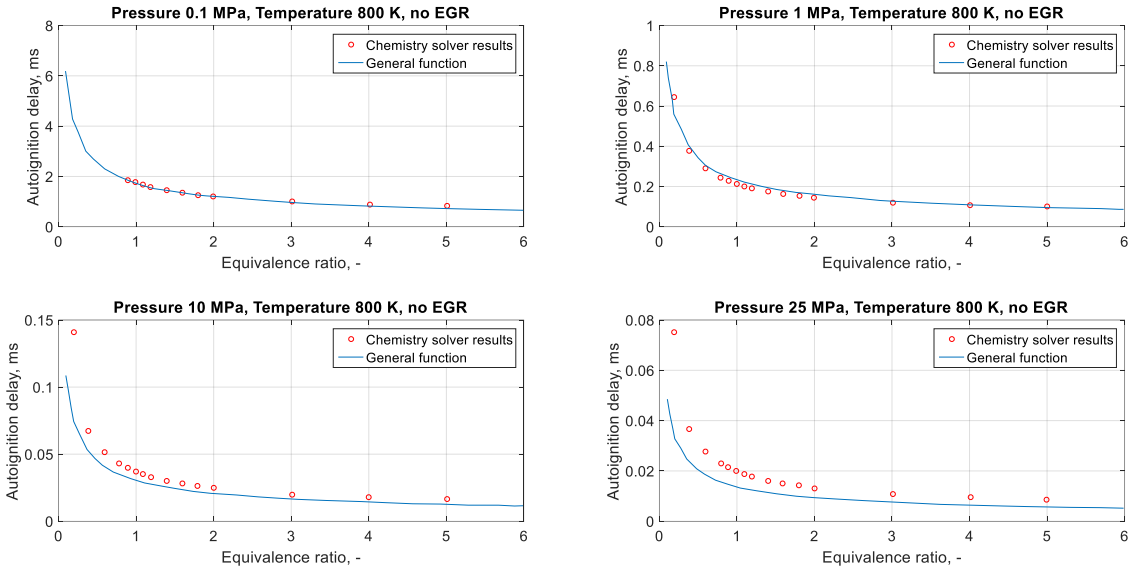

Figure 13 Chemistry solver results and autoignition results with the correlation function

In section 4., the operating conditions and numerical setup for the calculation are presented, for which the results are shown. The performed engine operating point features a multi-injection strategy of four separate injections, where the OME-3 fuel was injected at 20 °C. Figure 14 compares the most detailed chemistry mechanism of OME-3 fuel, Cai et al., and ECFM-3Z combustion model with implemented autoignition and laminar flame speed databases for two operating injection strategies shown in Table 4. A good trend was achieved for the temperature results, while the ignition timing was slightly delayed for the simulation of ECFM-3Z. That can also be attributed to the autoignition parameter for ECFM-3Z calculation, which was not calibrated but used as a default value of 1. The same ignition delay is observed for the rate of heat release results, while the peak of released heat is achieved with the same value. As seen from RoHR diagram, ECFM-3Z combustion is not so pronounced as with Cai et al. For the late-stage combustion, the biggest discrepancy is achieved, which can be mainly attributed to the simplified chemistry in the combustion model does not account for such detailed carbon-based reactions. A better agreement is reached for the single injection case than in a multi injection strategy with four different injections, which calculates autoignition delay based on the whole chemistry reactions

rather than on interpolated conditions based on four parameters from the generated database. The ECFM-3Z in combination with the developed method for database generation of autoignition and laminar flame speed has correctly described the ignition of each injection and its ignition and combustion process with significantly simpler chemistry and decreased computational demand. The computational discrepancy between the ECFM-3Z model and Cai et al. mechanism can be attributed mainly to the simplified chemistry description in the ECFM-3Z model, which accounts for transport equations for a dozen chemical species. In contrast, Cai accounts for transport equations for 322 chemical species. Finally, the computational time was decreased approximately 20 times with the ECFM-3Z model.

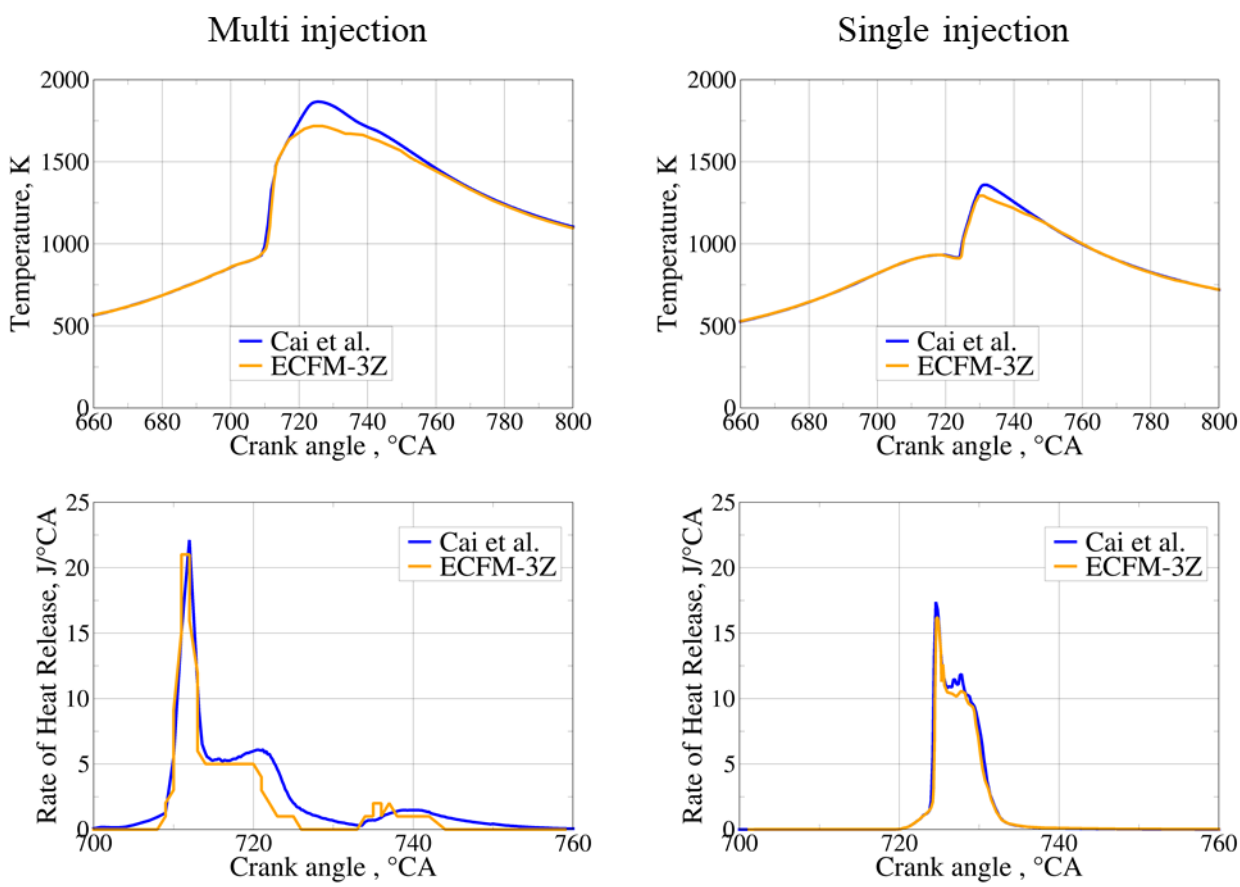

Figure 14 Comparison of temperature and rate of heat release results between detailed chemistry mechanism by Cai et al. and ECFM-3Z combustion model

6. CONCLUSIONS

The procedure of general functions for the generation of databases required for combustion modeling in the coherent flame models is developed in this work. The procedure is general and applicable to every fuel, and this work was mainly focused on the generation of laminar flame speed and autoignition databases for OME-3 fuel. Additionally, the developed procedure showed a good potential for reducing the number of required grid points since a reasonable agreement can be achieved with a few calculated points around stoichiometric values of equivalence ratio. The procedure validation was performed on generated laminar flame speed and autoignition database for OME-3 fuel, where a good agreement was achieved compared to the available experimental results. For the engine operating cycles, verification was made compared to the most detailed chemistry mechanism available in the literature, Cai et al. The verification results showed a great agreement in the trend and autoignition timing between mean in-cylinder temperature and rate of heat release curves for both single and multi injection strategy. In combination with coherent flame models, the developed method represents a robust and computationally low demanding procedure for accurate ignition and combustion process calculations of new biofuels and e-fuels. Although not presented in this work, the procedure was also developed for fuel blends, dual fuel, and multiple fuel combustion, where the additional fuel composition parameter was added as the fifth grid parameter. Therefore, the future work investigates the obtained databases for dual fuel and the impact of generated databases on the whole operating cycle in CFD software.

ACKNOWLEDGMENT

This work was funded under the auspice of the European Regional Development Fund, Operational Programme Competitiveness and Cohesion 2014−2020, KK.01.1.1.04.0070.

The Authors would wish to thank LOGEsoft™ for providing the software license through Academic Partner Program and for their support.

REFERENCES

[1] Stančin H, Mikulčić H, Wang X, Duić N. A review on alternative fuels in future energy system. Renew Sustain Energy Rev 2020;128:109927. doi:10.1016/j.rser.2020.109927.

[2] E J, Pham M, Zhao D, Deng Y, Le DH, Zuo W, et al. Effect of different technologies on combustion and emissions of the diesel engine fueled with biodiesel: A review. Renew Sustain Energy Rev 2017;80:620–47. doi:10.1016/j.rser.2017.05.250.

[3] Hänggi S, Elbert P, Bütler T, Cabalzar U, Teske S, Bach C, et al. A review of synthetic fuels for passenger vehicles. Energy Reports 2019;5:555–69. doi:10.1016/j.egyr.2019.04.007.

[4] Hossain A, Smith D, Davies P. Effects of Engine Cooling Water Temperature on Performance and Emission Characteristics of a Compression Ignition Engine Operated with Biofuel Blend. J Sustain Dev Energy, Water Environ Syst 2017;5:46–57. doi:10.13044/j.sdewes.d5.0132.

[5] Bešenić T, Mikulčić H, Vujanović M, Duić N. Numerical modelling of emissions of nitrogen oxides in solid fuel combustion. J Environ Manage 2018;215:177–84. doi:10.1016/j.jenvman.2018.03.014.

[6] Zhang Y, Zhong Y, Wang J, Tan D, Zhang Z, Yang D. Effects of Different Biodiesel-Diesel Blend Fuel on Combustion and Emission Characteristics of a Diesel Engine. Processes 2021;9:1984. doi:10.3390/pr9111984.

[7] Mikulčić H, Baleta J, Wang X, Wang J, Qi F, Wang F. Numerical simulation of ammonia/methane/air combustion using reduced chemical kinetics models. Int J Hydrogen Energy 2021;46:23548–63. doi:10.1016/j.ijhydene.2021.01.109.

[8] Geng L, Li S, Xiao Y, Xie Y, Chen H, Chen X. Effects of injection timing and rail pressure on combustion characteristics and cyclic variations of a common rail DI engine fuelled with F-T diesel synthesized from coal. J Energy Inst 2020;93:2148–62. doi:10.1016/j.joei.2020.05.009.

[9] Dirrenberger P, Glaude PA, Bounaceur R, Le Gall H, da Cruz AP, Konnov AA, et al. Laminar burning velocity of gasolines with addition of ethanol. Fuel 2014;115:162–9. doi:10.1016/j.fuel.2013.07.015.

[10] Davis GW. Addressing Concerns Related to the Use of Ethanol-Blended Fuels in Marine Vehicles. J Sustain Dev Energy, Water Environ Syst 2017;5:546–59. doi:10.13044/j.sdewes.d5.0175.

[11] Di Lorenzo M, Brequigny P, Foucher F, Mounaïm-Rousselle C. Validation of TRF-E as gasoline surrogate through an experimental laminar burning speed investigation. Fuel 2019;253:1578–88. doi:10.1016/j.fuel.2019.05.081.

[12] Hidegh G, Csemány D, Vámos J, Kavas L, Józsa V. Mixture Temperature-Controlled combustion of different biodiesels and conventional fuels. Energy 2021;234:121219. doi:10.1016/j.energy.2021.121219.

[13] Jurić F, Stipić M, Samec N, Hriberšek M, Honus S, Vujanović M. Numerical investigation of multiphase reactive processes using flamelet generated manifold approach and extended coherent flame combustion model. Energy Convers Manag 2021;240:114261. doi:10.1016/j.enconman.2021.114261.

[14] Colin O, Benkenida A. The 3-zones Extended Coherent Flame Model (ECFM3Z) for computing premixed/diffusion combustion. Oil Gas Sci Technol 2004;59:593–609. doi:10.2516/ogst:2004043.

[15] Mobasheri R. Analysis the ECFM-3Z Combustion Model for Simulating the Combustion Process and Emission Characteristics in a HSDI Diesel Engine. Int J Spray Combust Dyn

2015;7:353–71. doi:10.1260/1756-8277.7.4.353.

[16] Cai L, Jacobs S, Langer R, vom Lehn F, Heufer KA, Pitsch H. Auto-ignition of oxymethylene ethers (OMEn, n = 2–4) as promising synthetic e-fuels from renewable electricity: shock tube experiments and automatic mechanism generation. Fuel 2020;264:116711. doi:10.1016/j.fuel.2019.116711.

[17] Bradley D, Kalghatgi GT. Influence of autoignition delay time characteristics of different fuels on pressure waves and knock in reciprocating engines. Combust Flame 2009;156:2307–18. doi:10.1016/j.combustflame.2009.08.003.

[18] Wang W, Gowdagiri S, Oehlschlaeger MA. The high-temperature autoignition of biodiesels and biodiesel components. Combust Flame 2014;161:3014–21. doi:10.1016/j.combustflame.2014.06.009.

[19] Shahridzuan Abdullah I, Khalid A, Jaat N, Saputra Nursal R, Koten H, Karagoz Y. A study of ignition delay, combustion process and emissions in a high ambient temperature of diesel combustion. Fuel 2021;297:120706. doi:10.1016/j.fuel.2021.120706.

[20] Rajak U, Nashine P, Chaurasiya PK, Verma TN, Patel DK, Dwivedi G. Experimental & predicative analysis of engine characteristics of various biodiesels. Fuel 2021;285:119097. doi:10.1016/j.fuel.2020.119097.

[21] Rajak U, Nashine P, Dasore A, Balijepalli R, Kumar Chaurasiya P, Nath Verma T. Numerical analysis of performance and emission behavior of CI engine fueled with microalgae biodiesel blend. Mater Today Proc 2021. doi:10.1016/j.matpr.2021.02.104.

[22] Mullan Karishma S, Dasore A, Rajak U, Nath Verma T, Prahlada Rao K, Omprakash B. Experimental examination of CI engine fueled with various blends of diesel-apricot oil at different engine operating conditions. Mater Today Proc 2021. doi:10.1016/j.matpr.2021.02.105.

[23] Xuan T, Sun Z, EL-Seesy AI, Mi Y, Zhong W, He Z, et al. An optical study on spray

and combustion characteristics of ternary hydrogenated catalytic biodiesel/methanol/n-octanol blends; part I: Spray morphology, ignition delay, and flame lift-off length. Fuel 2021;289:119762. doi:10.1016/j.fuel.2020.119762.

[24] Kobashi Y, Todokoro M, Shibata G, Ogawa H, Mori T, Imai D. EGR gas composition effects on ignition delays in diesel combustion. Fuel 2020;281:118730. doi:10.1016/j.fuel.2020.118730.

[25] Lawson R, Gururajan V, Movaghar A, Egolfopoulos FN. Autoignition of reacting mixtures at engine-relevant conditions using confined spherically expanding flames. Proc Combust Inst 2021;38:2285–93. doi:10.1016/j.proci.2020.06.224.

[26] Rahnama P, Arab M, Reitz RD. A Time-Saving Methodology for Optimizing a Compression Ignition Engine to Reduce Fuel Consumption through Machine Learning. SAE Int J Engines 2020;13:03-13-02–0019. doi:10.4271/03-13-02-0019.

[27] Vignesh R, Ashok B. Deep neural network model-based global calibration scheme for split injection control map to enhance the characteristics of biofuel powered engine. Energy Convers Manag 2021;249:114875. doi:10.1016/j.enconman.2021.114875.

[28] Han W, Sun Z, Scholtissek A, Hasse C. Machine Learning of ignition delay times under dual-fuel engine conditions. Fuel 2021;288:119650. doi:10.1016/j.fuel.2020.119650.

[29] Misdariis A, Vermorel O, Poinsot T. A methodology based on reduced schemes to compute autoignition and propagation in internal combustion engines. Proc Combust Inst 2015;35:3001–8. doi:10.1016/j.proci.2014.06.053.

[30] Del Pecchia M, Breda S, D'Adamo A, Fontanesi S, Irimescu A, Merola S. Development of Chemistry-Based Laminar Flame Speed Correlation for Part-Load SI Conditions and Validation in a GDI Research Engine. SAE Int J Engines 2018;11:2018-01–0174. doi:10.4271/2018-01-0174.

[31] Del Pecchia M, Pessina V, Berni F, d'Adamo A, Fontanesi S. Gasoline-ethanol blend

formulation to mimic laminar flame speed and auto-ignition quality in automotive engines. Fuel 2020;264:116741. doi:10.1016/j.fuel.2019.116741.

[32] D'Adamo A, Del Pecchia M, Breda S, Berni F, Fontanesi S, Prager J. Chemistry-Based Laminar Flame Speed Correlations for a Wide Range of Engine Conditions for Iso-Octane, n-Heptane, Toluene and Gasoline Surrogate Fuels, 2017. doi:10.4271/2017-01-2190.

[33] Verhelst S, T′Joen C, Vancoillie J, Demuynck J. A correlation for the laminar burning velocity for use in hydrogen spark ignition engine simulation. Int J Hydrogen Energy 2011;36:957–74. doi:10.1016/j.ijhydene.2010.10.020.

[34] Ji C, Liu X, Wang S, Gao B, Yang J. Development and validation of a laminar flame speed correlation for the CFD simulation of hydrogen-enriched gasoline engines. Int J Hydrogen Energy 2013;38:1997–2006. doi:10.1016/j.ijhydene.2012.11.139.

[35] Liu X, Ji C, Gao B, Wang S, Liang C, Yang J. A laminar flame speed correlation of hydrogen–methanol blends valid at engine-like conditions. Int J Hydrogen Energy 2013;38:15500–9. doi:10.1016/j.ijhydene.2013.09.031.

[36] Cerinski D, Vujanović M, Petranović Z, Baleta J, Samec N, Hriberšek M. Numerical analysis of fuel injection configuration on nitrogen oxides formation in a jet engine combustion chamber. Energy Convers Manag 2020;220:112862. doi:10.1016/j.enconman.2020.112862.

[37] Colin O, Benkenida A. The 3-Zones Extended Coherent Flame Model \(Ecfm3z\) for Computing Premixed/Diffusion Combustion; The 3-Zones Extended Coherent Flame Model \(Ecfm3z\) for Computing Premixed/Diffusion Combustion 2004. doi:10.2516/ogst:2004043ï.

[38] Ren S, Wang Z, Li B, Liu H, Wang J. Development of a reduced polyoxymethylene dimethyl ethers (PODEn) mechanism for engine applications. Fuel 2019;238:208–24.

doi:10.1016/j.fuel.2018.10.111.

[39] Sun W, Wang G, Li S, Zhang R, Yang B, Yang J, et al. Speciation and the laminar burning velocities of poly(oxymethylene) dimethyl ether 3 (POMDME3) flames: An experimental and modeling study. Proc Combust Inst 2017;36:1269–78. doi:10.1016/j.proci.2016.05.058.

[40] Lin Q, Tay KL, Zhou D, Yang W. Development of a compact and robust Polyoxymethylene Dimethyl Ether 3 reaction mechanism for internal combustion engines. Energy Convers Manag 2019;185:35–43. doi:10.1016/j.enconman.2019.02.007.

[41] Gopinath S, Devan PK, Sabarish V, Sabharish Babu BV, Sakthivel S, Vignesh P. Effect of spray characteristics influences combustion in DI diesel engine – A review. Mater Today Proc 2020;33:52–65. doi:10.1016/j.matpr.2020.03.130.

[42] Gao H, Li X, Xue J, Bai H, He X, Liu F. A modification to the WAVE breakup model for evaporating diesel spray. Appl Therm Eng 2016;108:555–66. doi:10.1016/j.applthermaleng.2016.07.152.

[43] Abramzon B, Sirignano WA. Droplet vaporization model for spray combustion calculations. Int J Heat Mass Transf 1989;32:1605–18. doi:10.1016/0017-9310(89)90043-4.

[44] Gülder ÖL. Correlations of Laminar Combustion Data for Alternative S.I. Engine Fuels, 1984. doi:10.4271/841000.